TECHNICAL RESEARCH REPORT

Sampled-Data Modeling and Analysis of Closed-Loop PWM DC-DC Converters

by Chung-Chieh Fang, Eyad H. Abed

T.R. 99-24

Sampled-Data Modeling and Analysis of Closed-Loop PWM DC-DC Converters

Chung-Chieh Fang and Eyad H. Abed
Department of Electrical Engineering
and the Institute for Systems Research
University of Maryland
College Park, MD 20742 USA

Manuscript: February 1998; revised in March 1999

Abstract

Sampled-data analysis of converters has been a topic of investigation for the past two decades. However, this powerful tool is not widely used in control loop design or in closed-loop performance validation. Instead, averaged models are typically used for control loop design, while detailed simulations are used for validating closed-loop performance. This paper makes several contributions to the sampled-data modeling and analysis of *closed-loop* PWM DC-DC converters, with the aim of increasing appreciation and use of the method. General models are presented in a unified and simple manner, while removing simplifying approximations present in previous work. These models apply both for current mode control and voltage mode control. The general models are nonlinear. They are used to obtain *analytical* linearized models, which are in turn employed to obtain local stability results. Detailed examples illustrate the modeling and analysis in the paper, and point to situations in which the sampled-data approach gives results superior to alternate methods. For instance, it is shown that the sampled-data approach will reliably predict the (local) stability of a converter for which averaging or simulation predicts instability.

1 Introduction

Sampled-data analysis of converters has been a topic of investigation for the past two decades [1, 2, 3]. Sampled-data models of converters are accepted to be more accurate than their averaged counterparts. This can be important especially in studying dynamical behaviors that averaging is known not to capture well, such as subharmonic instability [4], chaotic phenomena [5, 6, 7, 8], and steady-state DC offset [9]. However, the powerful sampled-data approach is not widely used in control loop design or in closed-loop performance validation. Instead, averaged models are typically used for control loop design, while detailed simulations are used for validating closed-loop performance. This paper makes several contributions to the sampled-data modeling and analysis

of *closed-loop* PWM DC-DC converters, with the aim of increasing appreciation and use of the method. General models are presented in a unified and simple manner, while removing simplifying approximations present in previous work.

Because the dynamical behavior differs for continuous conduction mode (CCM) and discontinuous conduction mode (DCM), the general model in CCM differs from that in DCM. However, in either case the model applies both for current mode control and voltage mode control. Because of this, the modeling procedure presented here is considered to unify previous disparate contributions for current mode and voltage mode control.

The general models are nonlinear. They are used to obtain *analytical* linearized models, which are in turn employed to obtain local stability results. Detailed examples illustrate the modeling and analysis in the paper, and point to situations in which the sampled-data approach gives results superior to alternate methods. For instance, it is shown that the sampled-data approach will reliably predict the (local) stability of a converter for which averaging or simulation predicts instability.

It is important to clarify at the outset the differences between the contributions to modeling in this paper in relation to past contributions. In the next paragraph, the relation between the present work and the original work on sampled-data modeling and analysis of *closed-loop* PWM DC-DC converter operation is summarized. This is followed by a summary of the relation between this work and the literature on sampled-data modeling and analysis of the *power stage* of a PWM DC-DC converter.

Lee, Iwens, Yu and Triner [1] and Verghese, Elbuluk and Kassakian [2] are two seminal contributions to sampled-data modeling and analysis of DC-DC converters. These authors developed general models that apply to closed-loop converter operation. Thus, their results apply also to the modeling of the power stage of a converter. In relation to these papers, the present contribution gives more detail, unifies the modeling of current mode control and voltage mode control, and gives an *analytical* linearized sampled-data model (not given explicitly in the indicated references). In addition, the models given here incorporate the exact system trajectory between switching instants.

Tymerski [10, 11] developed general detailed sampled-data models of the *power stage* of a PWM

DC-DC converter. He also obtained an analytical linearized sampled-data model. These papers are similar to the present work, especially in that they reflect the exact trajectory between switching instants and include an analytical linearized sampled-data model. The main difference between the work in [10, 11] and the present paper is that here the *closed-loop* converter is considered, while in [10, 11] the *power stage* is considered.

The paper proceeds as follows. In Section 2, a general block diagram model valid in continuous conduction mode is given and used to obtain a nonlinear sampled-data model and an associated linearized model. The linearized model is used to study orbital stability, and to derive the audio-susceptibility and output impedance. In Section 3, analogous models are given for discontinuous conduction mode. In Section 4, four examples are given that illustrate application of the models of the paper to sample converter circuits. In addition, these examples demonstrate advantages of the sampled-data analysis over averaging and detailed simulation in validating closed-loop performance. Conclusions are collected in Section 5.

2 Continuous Conduction Mode (CCM)

2.1 Block Diagram Model

In this subsection, a block diagram model for the PWM converter in CCM is proposed. This model is shown to apply to current mode control and voltage mode control.

Consider, for example, a buck converter under current mode control and voltage mode control, shown in Fig. 1 and Fig. 2, respectively. They have different control schemes. However, they share the same characteristics: switching instants are determined by how a ramp signal $h(t)$ intersects with a feedback signal $y(t)$. This motivates a unified model for both current mode control and voltage mode control.

The proposed block diagram model for the PWM converter in CCM is shown in Fig. 3. In the diagram, $A_1, A_2 \in \mathbf{R}^{N\times N}$, $B_1, B_2 \in \mathbf{R}^{N\times 2}$, $C, E_1, E_2 \in \mathbf{R}^{1\times N}$, and $D \in \mathbf{R}$ are constant matrices, $x \in \mathbf{R}^N$, $y = Cx + Du \in \mathbf{R}$ are the state (of power stage and controller) and the feedback signal,

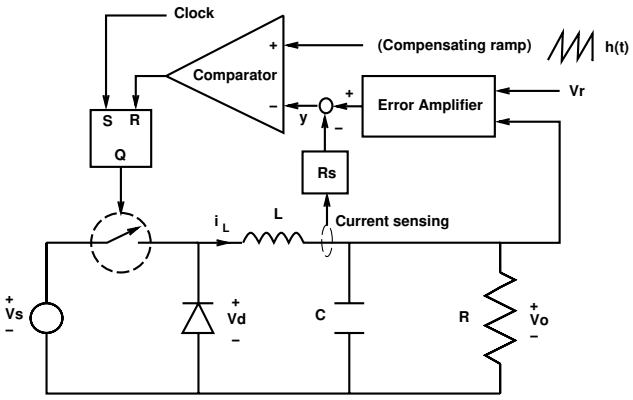

Figure 1: Buck converter under current mode control

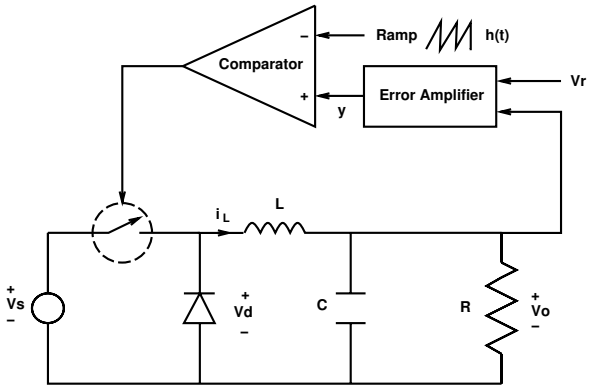

Figure 2: Buck converter under voltage mode control

respectively. The source voltage is v_s; the output voltage is v_o. The notation v_r denotes the reference signal, which could be a voltage or current reference. The reference signal v_r is allowed to be time-varying, although it is constant in most applications. The signal $h(t)$ is a T-periodic ramp with $h(0) = V_l$ and $h(T^-) = V_h$. The clock has the same frequency $f_s = 1/T$ as the ramp. This frequency is called the switching frequency. The two stages in each clock period in CCM are denoted by S_1 and S_2. The system is in S_1 immediatedly following a clock pulse, and switches to S_2 at instants $y(t) = h(t)$.

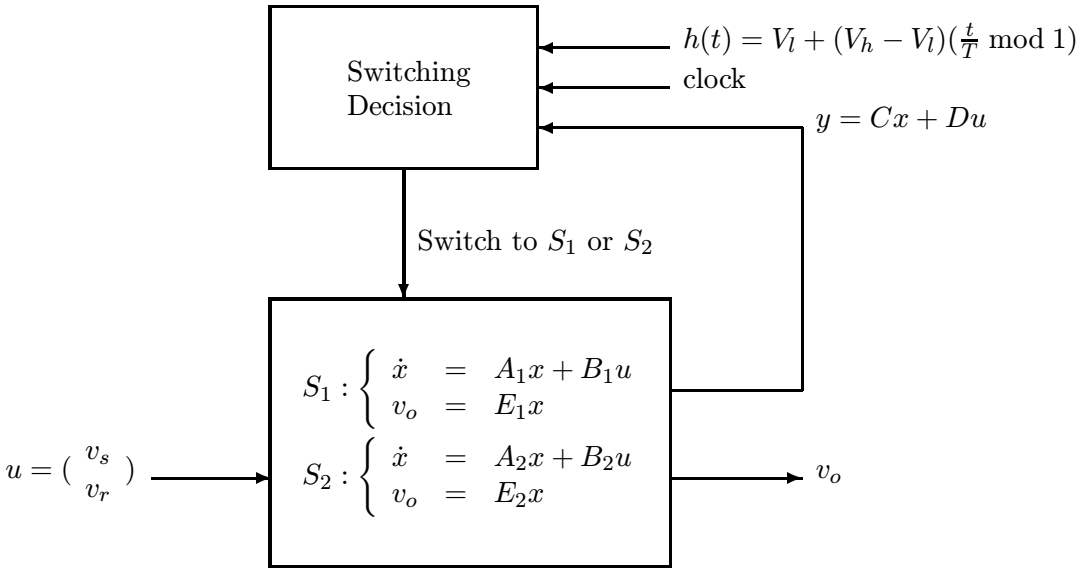

Figure 3: A block diagram model for PWM converters in CCM

Assume the switch and the diode in the PWM converter are ideal, so that there is no voltage drop when they are on. Most PWM converters can be modeled by Fig. 3. The PWM converter under current mode control fits this model exactly, with $h(t)$ denoting the slope-compensating ramp. For operation in voltage mode control, the system is switched between stages when the ramp signal $h(t)$ intersects with the feedback signal y. One of the switchings generally has the same frequency as the clock. Therefore the model in Fig. 3 is also good for the PWM converter under voltage mode control. Many other control schemes (e.g., average current mode control) also fit the model in Fig. 3. Typical waveforms in current and voltage mode control are shown in Fig. 4 and Fig. 5, respectively. Note that in Fig. 4, the ramp has positive slope, instead of negative slope

as commonly seen in most literatures, in order to be consistent with the case of voltage mode control.

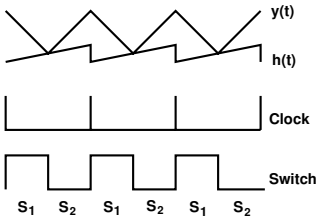

Figure 4: Waveforms of a PWM converter in CCM under current mode control

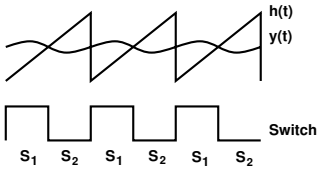

Figure 5: Waveforms of a PWM converter in CCM under voltage mode control

2.2 Nonlinear Sampled-Data Model

The switching action is essentially discrete. To arrive at a sampled-data model, the operation of the PWM converter within the cycle, $t \in [nT, (n+1)T)$, is considered. Generally in the PWM converter, the switching frequency is sufficiently high that the variations in v_s and v_r in a cycle can be neglected. Thus, take $u = (v_s, v_r)' \in \mathbf{R}^{2\times 1}$ to be constant within the cycle, and denote its value by $u_n = (v_{sn}, v_{rn})'$. (The notation v_{sn}, instead of $v_{s,n}$, is used for brevity. This applies to other variables.) Let $x_n = x(nT)$ and $v_{on} = v_o(nT)$. The sampled-data dynamics which maps x_n to x_{n+1} is derived next.

Denote by $nT + d_n$ the switching instant within the cycle when $y(t)$ and $h(t)$ intersect. Then $y(nT + d_n) = h(nT + d_n)$, and

$$S_1 \quad : \quad \left\{ \begin{array}{rcll} \dot{x} & = & A_1 x + B_1 u & \\ v_o & = & E_1 x & \end{array} \right. \qquad \text{for } t \in [nT, nT + d_n) \tag{1}$$

$$S_2 \quad : \quad \left\{ \begin{array}{rcl} \dot{x} & = & A_2 x + B_2 u \\ v_o & = & E_2 x \end{array} \right. \qquad \text{for } t \in [nT + d_n, (n+1)T) \tag{2}$$

The two matrices E_1 and E_2 need not be the same. For example, they can differ if the equivalent series resistance (ESR) $R_c \neq 0$. When they differ, the output voltage is discontinuous. An example of a discontinuous output voltage waveform is shown in Fig. 6. In most applications, the output voltage of interest is the maximum, minimum, or average voltage. So in the following, E is used to denote either E_1, E_2, or $(E_1 + E_2)/2$.

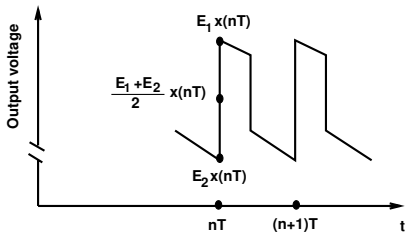

Figure 6: A discontinuous output voltage waveform

Using the dynamics (1) and (2) and the assumption that $u = (v_s, v_r)$ is constant within the cycle, one readily obtains the sampled-data dynamics (3)-(5) of the PWM converter in CCM. The dynamical equation (3) below is augmented with the constraint (4), corresponding to the intersection condition $y(nT + d_n) = h(nT + d_n)$ defining d_n.

$$\begin{aligned} x_{n+1} &= f(x_n, u_n, d_n) \\ &= e^{A_2(T-d_n)}(e^{A_1 d_n} x_n + \int_0^{d_n} e^{A_1(d_n-\sigma)} d\sigma B_1 u_n) + \int_{d_n}^{T} e^{A_2(T-\sigma)} d\sigma B_2 u_n \qquad (3) \\ g(x_n, u_n, d_n) &= y(nT + d_n) - h(nT + d_n) \\ &= C(e^{A_1 d_n} x_n + \int_0^{d_n} e^{A_1(d_n-\sigma)} d\sigma B_1 u_n) + D u_n - h(d_n) \\ &= 0 \qquad (4) \\ v_{on} &= E x_n \qquad (5) \end{aligned}$$

2.3 Steady-State Analysis

In the PWM converter, the steady-state operating condition is a *periodic solution*, not an equilibrium point as depicted in the averaging method. A T-periodic solution for system in Fig. 3 corresponds to a fixed point for the sampled-data model. A periodic solution $x^0(t)$ is sampled as $x^0(0)$. Let the fixed point in the sampled-data dynamics (3)-(5) be $(x_n, u_n, d_n) = (x^0(0), u, d)$, where $u = (V_s, V_r)'$. Then this fixed point satisfies

$$x^0(0) = f(x^0(0), u, d) \tag{6}$$

$$g(x^0(0), u, d) = 0 \tag{7}$$

where the functions $f(\cdot)$ and $g(\cdot)$ are given in Eqs. (3) and (4). These $N+1$ nonlinear equations (Eqs. (6) and (7)) in $N+1$ unknowns ($x^0(0)$ and d) can be solved by Newton's method [1]. After obtaining $x^0(0)$ and d, a periodic solution $x^0(t)$ is obtained:

$$x^0(t) = \begin{cases} e^{A_1 t}x^0(0) + \int_0^t e^{A_1(t-\sigma)}d\sigma B_1 u & \text{for } t \in [0, d) \\ e^{A_2(t-d)}x^0(d) + \int_d^t e^{A_2(t-\sigma)}d\sigma B_2 u & \text{for } t \in [d, T) \\ x^0(t \bmod T) & \text{for } t \geq T \end{cases} \tag{8}$$

A typical periodic solution $x^0(t)$ is shown Fig. 7. From Eqs. (1) and (2), $\dot{x}^0(d^-) = A_1 x^0(d) + B_1 u$ and $\dot{x}^0(d^+) = A_2 x^0(d) + B_2 u$.

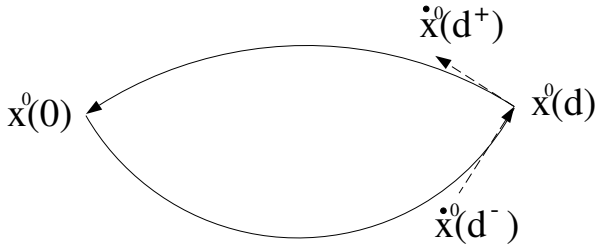

Figure 7: A typical periodic solution $x^0(t)$ of a PWM converter in state space

2.4 Existence of T-Periodic Solutions

Assume all of the eigenvalues of A_1 and A_2 are in the open left half of the complex plane, then the matrices $I - e^{A_2(T-d)}e^{A_1 d}$ and $I - e^{A_1 d}e^{A_2(T-d)}$ are invertible [12]. From Eq. (6), $x^0(0)$ can be

expressed as

$$x^0(0) \;=\; (I - e^{A_2(T-d)}e^{A_1 d})^{-1}(e^{A_2(T-d)}\int_0^d e^{A_1(d-\sigma)}d\sigma B_1 u + \int_d^T e^{A_2(T-\sigma)}d\sigma B_2 u) \tag{9}$$

Similarly, $x^0(d)$ can be expressed as a function of d, denoted as $X_s(d)$:

$$X_s(d) \;=\; (I - e^{A_1 d}e^{A_2(T-d)})^{-1}(e^{A_1 d}\int_d^T e^{A_2(T-\sigma)}d\sigma B_2 u + \int_0^d e^{A_1(d-\sigma)}d\sigma B_1 u) \tag{10}$$

The function $X_s(\cdot)$ has the following property:

$$X_s(0) \;=\; -A_2^{-1}B_2 u \tag{11}$$

$$X_s(T) \;=\; -A_1^{-1}B_1 u \tag{12}$$

So the $N+1$ equations, (6) and (7), reduce to one equation in one unknown d:

$$y(d) - h(d) = CX_s(d) + Du - h(d) = 0 \tag{13}$$

The next result gives a sufficient condition for existence of a fixed point in the sampled-data dynamics.

Theorem 1 *Assume that all of the eigenvalues of A_1 and A_2 are in the open left half of the complex plane. If*

$$(CA_2^{-1}B_2 u - Du + h(0))(CA_1^{-1}B_1 u - Du + h(T^-)) \le 0 \tag{14}$$

then there exists a fixed point $(x_n, u_n, d_n) = (x^0(0), u, d)$ in the sampled-data dynamics (3)-(5).

Proof: From Eq. (13), if

$$\begin{aligned}
&(y(0) - h(0))(y(T^-) - h(T^-)) \\
&\quad= (CX_s(0) + Du - h(0))(CX_s(T) + Du - h(T^-)) \\
&\quad= (CA_2^{-1}B_2 u - Du + h(0))(CA_1^{-1}B_1 u - Du + h(T^-)) \\
&\quad\le 0
\end{aligned}$$

then by the Intermediate Value Theorem, there exists a solution $d \in [0, T)$ satisfying Eq. (13). Hence there exists a fixed point $(x_n, u_n, d_n) = (x^0(0), u, d)$ in the sampled-data dynamics (3)-(5). □

Note: Whenever there exists a T-periodic solution for the system in Fig. 3, it will be found as a fixed point in the sampled-data model. However, a fixed point in the sampled-data model may not correspond to a T-periodic solution in Fig. 3. To explain the last remark, suppose a fixed point $(x_n, u_n, d_n) = (x^0(0), u, d)$ is obtained. Then a solution $x^0(t)$ can be obtained from Eq. (8). An example of signals $y^0(t) := Cx^0(t) + Du$ and $h(t)$ is shown in Fig. 8. The solution $y^0(t)$, although periodic with $y^0(d) = h(d)$, cannot be accepted because two switchings occur during $t \in (0, T)$.

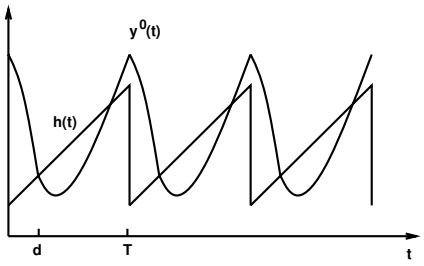

Figure 8: Ineligible signals $y^0(t)$ and $h(t)$ in voltage mode control

2.5 Linearized Sampled-Data Dynamics

The sampled-data dynamics (3)-(5) is constrained and nonlinear. Assuming that $\frac{\partial g}{\partial d_n} = C\dot{x}^0(d^-) - \dot{h}(d) \neq 0$, the Implicit Function Theorem allows one to linearize (3)-(5) at the fixed point $(x_n, u_n, d_n) = (x^0(0), u, d)$ to obtain an unconstrained linear sampled-data dynamical model. Using a hat $\hat{}$ to denote small perturbations (e.g., $\hat{x}_n = x_n - x^0(0)$), it follows that

$$\begin{array}{rcl} \hat{x}_{n+1} & \approx & \Phi\hat{x}_n + \Gamma\hat{u}_n \\ \hat{v}_{on} & = & E\hat{x}_n \end{array} \tag{15}$$

where

$$\Phi = \left. \frac{\partial f}{\partial x_n} - \frac{\partial f}{\partial d_n}\left(\frac{\partial g}{\partial d_n}\right)^{-1}\frac{\partial g}{\partial x_n} \right|_{(x_n,u_n,d_n)=(x^0(0),u,d)}$$

$$= e^{A_2(T-d)}(I - \frac{((A_1 - A_2)x^0(d) + (B_1 - B_2)u)C}{C(A_1x^0(d) + B_1u) - \dot{h}(d)})e^{A_1 d}$$

$$= e^{A_2(T-d)}(I - \frac{(\dot{x}^0(d^-) - \dot{x}^0(d^+))C}{C\dot{x}^0(d^-) - \dot{h}(d)})e^{A_1 d} \quad (16)$$

$$\Gamma = \frac{\partial f}{\partial u_n} - \frac{\partial f}{\partial d_n}(\frac{\partial g}{\partial d_n})^{-1}\frac{\partial g}{\partial u_n}\Big|_{(x_n,u_n,d_n)=(x^0(0),u,d)}$$

$$= e^{A_2(T-d)}(\int_0^d e^{A_1\sigma}d\sigma B_1 - \frac{\dot{x}^0(d^-) - \dot{x}^0(d^+)}{C\dot{x}^0(d^-) - \dot{h}(d)}(C\int_0^d e^{A_1\sigma}d\sigma B_1 + D)) + \int_0^{T-d} e^{A_2\sigma}d\sigma B_2 \quad (17)$$

Recall that $u_n = (v_{sn}, v_{rn})'$, and denote $\Gamma = [\Gamma_1, \Gamma_2]$. Eq. (15) can be rewritten as

$$\begin{array}{lcl} \hat{x}_{n+1} & \approx & \Phi\hat{x}_n + \Gamma_1\hat{v}_{sn} + \Gamma_2\hat{v}_{rn} \\ \hat{v}_{on} & = & E\hat{x}_n \end{array} \quad (18)$$

2.6 Stability Analysis

The relevant stability notion is *asymptotic orbital stability*, not asymptotic stability of an equilibrium point as depicted in the averaging method. In the power electronics literature, the PWM converter is generally said to be either stable or unstable, without mentioning orbital stability per se. The definition of asymptotic orbital stability is given as follows.

Definition 1 *(see, e.g., [13]) Denote by γ the closed orbit generated by the periodic solution $x^0(t)$. Then $x^0(t)$ is asymptotically orbitally stable if there is a δ such that*

$$\text{dist}[x(0), \gamma] < \delta \Rightarrow \lim_{t\to\infty} \text{dist}[x(t), \gamma] = 0$$

where $\text{dist}[z, \gamma]$ *is defined as the smallest distance between the point z and any point on γ.*

The orbital stability is related to the the set of eigenvalues of Φ, denoted by $\sigma[\Phi]$. Recall the following basic results on asymptotic orbital stability of the periodic solution $x^0(t)$.

Theorem 2 *[13] The fixed point $x^0(0)$ of the system (3)-(5) is asymptotically stable, or equivalently the periodic solution $x^0(t)$ in the original continuous-time system of Fig. 3 is asymptotically orbitally*

stable if all of the eigenvalues of Φ *are inside the unit circle of the complex plane. Moreover, if* $x^0(t)$ *is asymptotically orbitally stable, then no eigenvalues of* Φ *lies outside the unit circle.*

The following well known fact from linear algebra [14, p. 667] will be used in the proofs below.

Lemma 1 *If* A *and* B *are conformable rectangular matrices, then*

$$\det[I + AB] = \det[I + BA]$$

The preceding theorem and lemma will be used to show the following.

Theorem 3 *If the periodic solution* $x^0(t)$ *is asymptotically orbitally stable, then the following inequality holds:*

$$\left| \frac{C\dot{x}^0(d^+) - \dot{h}(d)}{C\dot{x}^0(d^-) - \dot{h}(d)} \right| \leq e^{\mathrm{tr}[A_2 - A_1]d - \mathrm{tr}[A_2]T} \tag{19}$$

Equivalently, if (19) does not hold, then the periodic solution $x^0(t)$ *is not asymptotically orbitally stable.*

Proof: Suppose the periodic solution $x^0(t)$ is asymptotically orbitally stable. Then all the eigenvalues of Φ have magnitude less than or equal than 1. Since $\det[\Phi]$ is the product of the eigenvalues of Φ, it follows that

$$\begin{aligned}
|\det[\Phi]| &= \left| \det[e^{A_1 d} e^{A_2(T-d)}] \det[I - \frac{(\dot{x}^0(d^-) - \dot{x}^0(d^+))C}{C\dot{x}^0(d^-) - \dot{h}(d)}] \right| \\
&= \left| \det[e^{A_1 d} e^{A_2(T-d)}] \det[1 - \frac{C(\dot{x}^0(d^-) - \dot{x}^0(d^+))}{C\dot{x}^0(d^-) - \dot{h}(d)}] \right| \\
&= e^{-\mathrm{tr}[A_2 - A_1]d + \mathrm{tr}[A_2]T} \left| \frac{C\dot{x}^0(d^+) - \dot{h}(d)}{C\dot{x}^0(d^-) - \dot{h}(d)} \right| \\
&\leq 1
\end{aligned}$$

where the second line of the calculation follows from Lemma 1. □

Remark: Inequality (19) is a necessary (but not sufficient) condition for stability. Generally the switching period is so small that the right side of (19) can be approximated as 1, resulting in a condition that resembles a well-known stability criterion in current mode control [15, for example]:

$$\left|\frac{m_2 - m_c}{m_1 - m_c}\right| < 1 \tag{20}$$

where m_1 is the (positive) slope of the *inductor current* trajectory during the on stage and m_2 is the (negative) slope during the off stage using a *linear approximation* [16]; and m_c is the (negative) slope of the compensating ramp. (Note that here $m_1 > 0$, $m_2 < 0$ and $m_c \leq 0$, which differs from most literatures' notations: $m_1 > 0$, $m_2 > 0$ and $m_c \geq 0$.) Theorem 3 differs from (20) in its use of instantaneous, rather than approximate, slope. Also, $Cx^0(t)$ in Theorem 3 is composed of more state signals (up to N) than just inductor current.

The next result asserts that a closed-loop pole is zero if the ramp has slope $C\dot{x}^0(d^+) = C(A_2x^0(d) + B_2u)$.

Theorem 4 *If the ramp slope $\dot{h}(d) = C\dot{x}^0(d^+)$, then the matrix Φ has a zero eigenvalue.*

Proof: From the proof in Theorem 3, it can be seen that if $\dot{h}(d) = C\dot{x}^0(d^+)$, then $\det[\Phi] = 0$ and hence the matrix Φ has a zero eigenvalue. □

Remark: Generally, a ramp with slope $C\dot{x}^0(d^+)$ is considered to produce deadbeat behavior (finite settling time) [15, p. 418]. This requires all of the N closed-loop poles to be at 0. Theorem 4 predicts that if the ramp has slope $C\dot{x}^0(d^+)$, then one eigenvalue is 0. Indeed, examples can be constructed showing that not necessarily all the eigenvalues vanish. Deadbeat behavior is therefore not guaranteed.

Theorem 5 and Corollary 2 below address the case in which the switching frequency goes to infinity. The following corollary of Lemma 1 is used in the proof of Theorem 5.

Corollary 1 *Let a and b be column vectors of the dimension N. Then one eigenvalue of the square matrix ab' is $b'a$, and the remaining $N-1$ eigenvalues are zero.*

Proof:

$$\begin{aligned}
\det[\lambda I - ab'] &= \lambda^N \det[I - \frac{ab'}{\lambda}] && (21)\\
&= \lambda^N \det[1 - \frac{b'a}{\lambda}] && (22)\\
&= \lambda^N (1 - \frac{b'a}{\lambda}) && (23)\\
&= \lambda^{N-1}(\lambda - b'a), && (24)
\end{aligned}$$

where the second line follows from Lemma 1. □

Theorem 5 *As the switching frequency f_s goes to infinity, an eigenvalue of Φ asymptotically approaches $\frac{C\dot{x}^0(d^+)-\dot{h}(d)}{C\dot{x}^0(d^-)-\dot{h}(d)}$ and the remaining $(N-1)$ eigenvalues approach 1.*

Proof: As the switching frequency f_s goes to infinity, both $e^{A_2(T-d)}$ and $e^{A_1 d}$ approach identity matrices. Eq. (16) now implies that Φ approaches $(I - \frac{(\dot{x}^0(d^-)-\dot{x}^0(d^+))C}{C\dot{x}^0(d^-)-\dot{h}(d)})$. Note that the matrix $(\dot{x}^0(d^-)-\dot{x}^0(d^+))C$ is the product of a column vector and a row vector, so that Corollary 1 applies. Thus this matrix has an eigenvalue at $C(\dot{x}^0(d^-)-\dot{x}^0(d^+))$ and $(N-1)$ eigenvalues at 0. This in turn implies that the matrix $I - \frac{(\dot{x}^0(d^-)-\dot{x}^0(d^+))C}{C\dot{x}^0(d^-)-\dot{h}(d)}$ has an eigenvalue at $1 - \frac{C(\dot{x}^0(d^-)-\dot{x}^0(d^+))}{C\dot{x}^0(d^-)-\dot{h}(d)} = \frac{C\dot{x}^0(d^+)-\dot{h}(d)}{C\dot{x}^0(d^-)-\dot{h}(d)}$ and $(N-1)$ eigenvalues at 1. □

Remark: Generally the averaged model is reliable for sufficiently high switching frequency [9]. This theorem implies that the stability criterion in (20) does indeed provide a *necessary* condition for stability when the switching frequency is sufficiently high.

Corollary 2 *Assume the switching frequency goes to infinity and $C\dot{x}^0(d^-) < \dot{h}(d)$ (which is generally true). If (i) $C\dot{x}^0(d^+) < C\dot{x}^0(d^-)$ or (ii) $\dot{h}(d) < \frac{C(\dot{x}^0(d^+)+\dot{x}^0(d^-))}{2}$, then the system is not asymptotically stable.*

Proof: Under the stated assumptions, it can be proved that the eigenvalue $\frac{C\dot{x}^0(d^+)-\dot{h}(d)}{C\dot{x}^0(d^-)-\dot{h}(d)}$ is greater than 1 under condition (i), or less than -1 under condition (ii). Thus, the system is not asymptot-

ically stable. □

Remark: The corollary asserts that if the switching frequency is high and if the slopes of the output variable $\dot{y} = C\dot{x}$ are not properly set in the design (condition (i)) or if the ramp slope is not large enough (condition (ii)), the system will be unstable.

2.7 Comparison with Stability Analysis Using State-Space Averaging

The duty cycle changes from cycle to cycle. This variable determines when the switch is on or off, and it is crucial in the system dynamics. So this variable needs to be modeled properly. The averaging method, however, treats the duty cycle as a continuous-time variable.

Next, stability analysis using the averaging method is briefly summarized. For details, the reader is referred to [15]. Let the duty cycle in the averaging method be d_c, with nominal value D_c. Also let

$$A_{\text{ave}} := A_{\text{ON}}D_c + A_{\text{OFF}}(1 - D_c) \tag{25}$$

$$B_{\text{ave}} := B_{\text{ON}}D_c + B_{\text{OFF}}(1 - D_c) \tag{26}$$

$$E_{\text{ave}} = E_{\text{ON}}D_c + E_{\text{OFF}}(1 - D_c) \tag{27}$$

$$X_{\text{ave}} = -A_{\text{ave}}^{-1}B_{\text{ave}}V_s \tag{28}$$

The nominal solution by the averaging method is X_{ave}, a constant instead of a periodic solution $x^0(t)$. Linearized around the nominal operating point $(x, u, d_c) = (X_{\text{ave}}, (V_s, V_r)', D_c)$, the system in Fig. 3 has the following linearized *continuous-time* dynamics

$$\dot{\hat{x}} \approx A_{\text{ave}}\hat{x} + B_{\text{ave}}\hat{u} + ((A_{\text{ON}} - A_{\text{OFF}})X_{\text{ave}} + (B_{\text{ON}} - B_{\text{OFF}})u)\hat{d}_c \tag{29}$$

$$\hat{y} = C\hat{x} + D\hat{u} \tag{30}$$

$$\hat{v}_o = E_{\text{ave}}\hat{x} + (E_{\text{ON}} - E_{\text{OFF}})\hat{d}_c \tag{31}$$

with

$$\hat{d}_c = \begin{cases} \frac{\hat{y}}{V_h - V_l} = \frac{\hat{y}}{h(d)T} & \text{(for trailing-edge modulation, because } d_c = \frac{y - V_l}{V_h - V_l}\text{)} \\ \frac{-\hat{y}}{V_h - V_l} = \frac{-\hat{y}}{h(d)T} & \text{(for leading-edge modulation, because } d_c = \frac{V_h - y}{V_h - V_l}\text{)} \end{cases} \tag{32}$$

In either trailing-edge modulation (S_1: switch on, S_2: off) or leading-edge modulation (S_1: off, S_2: on), Substituting Eqs. (29) and (32) into Eq. (29) gives

$$\dot{\hat{x}} \approx \mathcal{A}\hat{x} + \mathcal{B}\hat{u} \tag{33}$$

where (stage S_1 or S_2 can be either on or off stage)

$$\mathcal{A} = A_{\text{ave}} + ((A_1 - A_2)X_{\text{ave}} + (B_1 - B_2)u)\frac{C}{\dot{h}(d)T} \tag{34}$$

$$\mathcal{B} = B_{\text{ave}} + ((A_1 - A_2)X_{\text{ave}} + (B_1 - B_2)u)\frac{D}{\dot{h}(d)T} \tag{35}$$

The system is asymptotically stable if all of the eigenvalues of $\mathcal{A}$ are in the open left half of the complex plane, which is equivalent to all of the eigenvalues of $\exp(\mathcal{A}T)$ being inside the unit circle. From Eq. (34), $\exp(\mathcal{A}T)$ can be written as (for either trailing-edge or leading-edge modulation)

$$\exp(\mathcal{A}T) = e^{A_2(T-d)+A_1 d+\frac{((A_1-A_2)X_{\text{ave}}+(B_1-B_2)u)C}{\dot{h}(d)}} \tag{36}$$

which is similar in form to Φ in Eq. (16).

Comparing Eqs. (36) and (16), it is seen that the averaging method agrees with the sampled-data method under the following conditions:

1. $x^0(d)$ is approximated by X_{ave} (true if the periodic solution $x^0(t)$ is approximated by the equilibrium X_{ave}).

2. $C\dot{x}^0(d^-)$ is much smaller than $\dot{h}(d)$.

3. T is very small, so that $e^{(\dot{x}^0(d^-)-\dot{x}^0(d^+))CT} \approx I + (\dot{x}^0(d^-) - \dot{x}^0(d^+))CT$.

4. The matrices A_1, A_2 and $(\dot{x}^0(d^-) - \dot{x}^0(d^+))C$ commute.

Note that condition 4 is unlikely to hold, and condition 2 generally does not hold for current mode control.

2.8 Closed-Loop Audio-Susceptibility and Output Impedance

Audio-Susceptibility and output impedance are expressed in terms of transfer functions (frequency responses). They give information on the effect of (source or load) disturbances at various frequen-

cies on the output voltage.

The audio-susceptibility is derived directly from the linearized sampled-data model, Eq. (18). It is

$$T_{os}(z) = \frac{\hat{v}_o(z)}{\hat{v}_s(z)} = E(zI - \Phi)^{-1}\Gamma_1 \tag{37}$$

To calculate the output impedance, add a fictitious current source i_o (as perturbation) in parallel with the load. Then the state equations in Eqs. (1) and (2) are replaced by

$$S_1 : \dot{x} = A_1 x + B_{11} v_s + B_{12} v_r + B_{13} i_o \tag{38}$$

$$S_2 : \dot{x} = A_2 x + B_{21} v_s + B_{22} v_r + B_{23} i_o \tag{39}$$

where $B_{13}, B_{23} \in \mathbf{R}^{N\times 1}$.

Since i_o is used as perturbation, the nominal value of i_o is 0. Similar to the derivation in Section 2.2, the new linearized sampled-data dynamics is

$$\begin{array}{lcl} \hat{x}_{n+1} & \approx & \Phi\hat{x}_n + \Gamma_1\hat{v}_{sn} + \Gamma_2\hat{v}_{rn} + \Gamma_3\hat{i}_{on} \\ \hat{v}_{on} & = & E\hat{x}_n \end{array} \tag{40}$$

where

$$\begin{aligned} \Gamma_3 &= \frac{\partial f}{\partial i_{on}} - \frac{\partial f}{\partial d_n}\left(\frac{\partial g}{\partial d_n}\right)^{-1}\frac{\partial g}{\partial i_{on}}\bigg|_{(x_n,u,d_n,i_{on})=(x^0(0),u,d,0)} \\ &= e^{A_2(T-d)}\left(\int_0^d e^{A_1\sigma}d\sigma B_{13} - \frac{\dot{x}^0(d^-) - \dot{x}^0(d^+)}{C\dot{x}^0(d^-) - \dot{h}(d)} C\int_0^d e^{A_1\sigma}d\sigma B_{13}\right)\int_0^{T-d} e^{A_2\sigma}d\sigma B_{23} \end{aligned} \tag{41}$$

and i_{on} is the sampled perturbed output current. So the output impedance is

$$T_{oo}(z) = \frac{\hat{v}_o(z)}{\hat{i}_o(z)} = E(zI - \Phi)^{-1}\Gamma_3 \tag{42}$$

Given a transfer function in z domain, say $T(z)$, its effective frequency response [17, p. 93] is $T(e^{j\omega T})$, which is valid in the frequency range $|\omega| < \frac{\pi}{T}$.

3 Discontinuous Conduction Mode (DCM)

3.1 Block Diagram Model

There are three stages in DCM in a cycle. The first two stages and their operation are the same as in CCM. The system is switched to the third stage when the inductor current i_L reaches zero. Within the third stage, $i_L = 0$. A block diagram model for the PWM converter in DCM is shown in Fig. 9. The matrix $F \in \mathbf{R}^{1\times N}$ is chosen such that $Fx = i_L$. The remaining notation is the same as in Fig. 3.

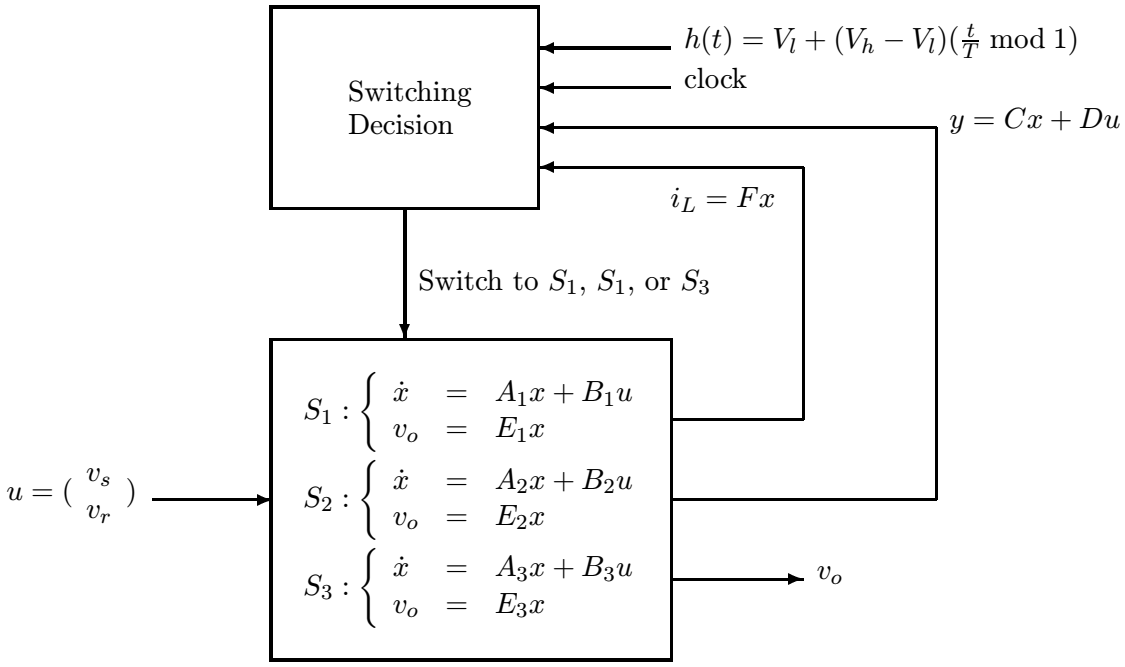

Figure 9: A block diagram model for PWM converters in DCM

3.2 Nonlinear Sampled-Data Model

Consider the operation of the PWM converter within the cycle, $t \in [nT, (n+1)T)$. As in CCM, take $u = (v_s, v_r)'$ to be constant within the cycle and denote its value by $u_n = (v_{sn}, v_{rn})'$.

Denote by $nT + d_{1n}$ the switching instant when $y(t)$ and $h(t)$ intersect within the cycle. (The notation d_{1n}, instead of $d_{1,n}$, is used for brevity.) Denote by $nT + d_{2n}$ the switching instant when

the inductor current reaches zero. The three stages S_1, S_2, S_3 within the cycle are thus

$$S_1 \ : \ \left\{ \begin{array}{rcll} \dot{x} & = & A_1 x + B_1 u & \\ v_o & = & E_1 x & \end{array} \right. \qquad \text{for } t \in [nT, nT + d_{1n}) \tag{43}$$

$$S_2 \ : \ \left\{ \begin{array}{rcll} \dot{x} & = & A_2 x + B_2 u & \\ v_o & = & E_2 x & \end{array} \right. \qquad \text{for } t \in [nT + d_{1n}, nT + d_{2n}) \tag{44}$$

$$S_3 \ : \ \left\{ \begin{array}{rcll} \dot{x} & = & A_3 x + B_3 u & \\ v_o & = & E_3 x & \end{array} \right. \qquad \text{for } t \in [nT + d_{2n}, (n+1)T) \tag{45}$$

The two switching conditions (at $t = nT + d_{1n}$ and $nT + d_{2n}$) are

$$y(nT + d_{1n}) \ = \ Cx(nT + d_{1n}) + Du_n = h(nT + d_{1n}) \tag{46}$$

$$i_L(nT + d_{2n}) \ = \ Fx(nT + d_{2n}) = 0 \tag{47}$$

As in CCM, the output voltage in DCM can be discontinuous at the clock time. Again, E is used to denote E_1, E_3, or $(E_1 + E_3)/2$ depending on which value of output voltage is of interest.

From Eqs. (43)-(47), the PWM converter in DCM has the following sampled-data dynamics:

$$\begin{aligned} x_{n+1} \ &= \ f(x_n, u_n, d_n) \\ &= \ e^{A_3(T-d_{2n})}(e^{A_2(d_{2n}-d_{1n})}(e^{A_1 d_{1n}} x_n + \int_0^{d_{1n}} e^{A_1(d_{1n}-\sigma)} d\sigma B_1 u_n) \\ &\quad + \int_{d_{1n}}^{d_{2n}} e^{A_2(d_{2n}-\sigma)} d\sigma B_2 u_n) + \int_{d_{2n}}^{T} e^{A_3(T-\sigma)} d\sigma B_3 u_n \end{aligned} \tag{48}$$

$$v_{on} \ = \ Ex_n \tag{49}$$

$$\begin{aligned} g(x_n, u_n, d_n) \ &= \ \left[\begin{array}{c} Cx(nT + d_{1n}) + Du_n - h(nT + d_{1n}) \\ Fx(nT + d_{2n}) \end{array} \right] \\ &= \ \left[\begin{array}{c} C(e^{A_1 d_{1n}} x_n + \int_0^{d_{1n}} e^{A_1 \sigma} d\sigma B_1 u_n) + Du_n - h(d_{1n}) \\ F(e^{A_2(d_{2n}-d_{1n})}(e^{A_1 d_{1n}} x_n + \int_0^{d_{1n}} e^{A_1 \sigma} d\sigma B_1 u_n) + \int_0^{d_{2n}-d_{1n}} e^{A_2 \sigma} d\sigma B_2 u_n) \end{array} \right] \\ &= \ 0 \end{aligned} \tag{50}$$

where $d_n = (d_{1n}, d_{2n})'$. Since the inductor current always starts from 0 at the beginning of a cycle, another explicit constraint is $Fx_n = i_{Ln} = 0$, for *any* n. So the dynamics is (N-1)-dimensional

instead of N-dimensional.

3.3 Linearized Sampled-Data Dynamics

Linearizing Eqs. (48)-(50) and using the notation $\diamond$ to denote evaluation at the fixed point $(x_n, u_n, d_n) = (x^0(0), u, (d_1, d_2)')$, one has

$$\begin{array}{rcl} \hat{x}_{n+1} & \approx & \Phi\hat{x}_n + \Gamma\hat{u}_n \\ \hat{v}_{on} & = & E\hat{x}_n \end{array} \tag{51}$$

where

$$\Phi = \frac{\partial f}{\partial x_n} - \frac{\partial f}{\partial d_n}(\frac{\partial g}{\partial d_n})^{-1}\frac{\partial g}{\partial x_n}\Big|_\diamond \tag{52}$$

$$\Gamma = \frac{\partial f}{\partial u_n} - \frac{\partial f}{\partial d_n}(\frac{\partial g}{\partial d_n})^{-1}\frac{\partial g}{\partial u_n}\Big|_\diamond \tag{53}$$

$$\frac{\partial f}{\partial x_n}\Big|_\diamond = e^{A_3(T-d_2)}e^{A_2(d_2-d_1)}e^{A_1 d_1} \tag{54}$$

$$\frac{\partial f}{\partial d_n}\Big|_\diamond = e^{A_3(T-d_2)}\left[\begin{array}{cc} e^{A_2(d_2-d_1)}(\dot{x}^0(d_1^-) - \dot{x}^0(d_1^+)) & \dot{x}^0(d_2^-) - \dot{x}^0(d_2^+) \end{array}\right] \tag{55}$$

$$\frac{\partial g}{\partial d_n}\Big|_\diamond = \left[\begin{array}{cc} C\dot{x}^0(d_1^-) - \dot{h}(d_1) & 0 \\ Fe^{A_2(d_2-d_1)}(\dot{x}^0(d_1^-) - \dot{x}^0(d_1^+)) & F\dot{x}^0(d_2^-) \end{array}\right] \tag{56}$$

$$\frac{\partial g}{\partial x_n}\Big|_\diamond = \left[\begin{array}{c} C \\ Fe^{A_2(d_2-d_1)} \end{array}\right] e^{A_1 d_1} \tag{57}$$

$$\frac{\partial f}{\partial u_n}\Big|_\diamond = e^{A_3(T-d_2)}(e^{A_2(d_2-d_1)}\int_0^{d_1} e^{A_1\sigma}d\sigma B_1 + \int_0^{d_2-d_1} e^{A_2\sigma}d\sigma B_2) + \int_0^{T-d_2} e^{A_3\sigma}d\sigma B_3 \tag{58}$$

$$\frac{\partial g}{\partial u_n}\Big|_\diamond = \left[\begin{array}{c} C\int_0^{d_1} e^{A_1\sigma}d\sigma B_1 + D \\ F(e^{A_2(d_2-d_1)}\int_0^{d_1} e^{A_1\sigma}d\sigma B_1 + \int_0^{d_2-d_1} e^{A_2\sigma}d\sigma B_2) \end{array}\right] \tag{59}$$

Since the inductor current i_L starts at 0 and ends at 0 in any cycle, it is not a dynamic variable. Thus, the dimension of the dynamics can be reduced by one. Note that this also implies that Φ possesses a zero eigenvalue, i.e. that $\det[\Phi] = 0$. This is shown in detail as follows:

$$\det[\Phi] = \det[e^{A_3(T-d_2)}e^{A_2(d_2-d_1)}(I - \left[\begin{array}{cc} \dot{x}^0(d_1^-) - \dot{x}^0(d_1^+) & e^{-A_2(d_2-d_1)}(\dot{x}^0(d_2^-) - \dot{x}^0(d_2^+)) \end{array}\right] \cdot$$

$$
\begin{aligned}
& (\frac{\partial g}{\partial d_n})^{-1}\Big|_{\diamond} \begin{bmatrix} C \\ Fe^{A_2(d_2-d_1)} \end{bmatrix}) e^{A_1 d_1}] \\
= \;& \det[e^{A_1 d_1} e^{A_3(T-d_2)} e^{A_2(d_2-d_1)}] \det[I - \begin{bmatrix} C \\ Fe^{A_2(d_2-d_1)} \end{bmatrix} \cdot \\
& \begin{bmatrix} \dot{x}^0(d_1^-) - \dot{x}^0(d_1^+) & e^{-A_2(d_2-d_1)}(\dot{x}^0(d_2^-) - \dot{x}^0(d_2^+)) \end{bmatrix} (\frac{\partial g}{\partial d_n})^{-1}\Big|_{\diamond}] \\
= \;& \det[e^{A_1 d_1} e^{A_3(T-d_2)} e^{A_2(d_2-d_1)}] \cdot \\
& \det[I - \begin{bmatrix} C(\dot{x}^0(d_1^-) - \dot{x}^0(d_1^+)) & Ce^{-A_2(d_2-d_1)}(\dot{x}^0(d_2^-) - \dot{x}^0(d_2^+)) \\ Fe^{A_2(d_2-d_1)}(\dot{x}^0(d_1^-) - \dot{x}^0(d_1^+)) & F\dot{x}^0(d_2^-) \end{bmatrix} \cdot \\
& \frac{\begin{bmatrix} F\dot{x}^0(d_2^-) & 0 \\ -Fe^{A_2(d_2-d_1)}(\dot{x}^0(d_1^-) - \dot{x}^0(d_1^+)) & C\dot{x}^0(d_1^-) - \dot{h}(d_1) \end{bmatrix}}{(C\dot{x}^0(d_1^-) - \dot{h}(d_1))F\dot{x}^0(d_2^-)}] \\
= \;& \det[e^{A_1 d_1} e^{A_3(T-d_2)} e^{A_2(d_2-d_1)}] \det[I - \begin{bmatrix} * & * \\ 0 & 1 \end{bmatrix}] \\
= \;& 0
\end{aligned}
$$

here $*$ signifies an irrelevant term.

The stability, audio-susceptibility and output impedance analysis are similar to the case in CCM and are omitted.

4 Illustrative Examples

Example 1 (*Local vs. global orbital stability*, [9, p. 90]) Consider the boost converter shown in Fig. 10, where $T = 2\mu s$, $V_s = 4V$, $L = 5.24\mu H$, $C = 0.2\mu F$, $R = 16\Omega$, $k_1 = -0.1$, $k_2 = 0.01$, $V_r = 0.48V$, and $h(t) = ((\frac{t}{T}) \mod 1)$.

Although the control scheme is neither voltage nor current mode control, the circuit can still be expressed in terms of the block diagram model in Fig. 3, with state $x = (i_L, v_C)'$:

$$
\begin{aligned}
A_1 &= \begin{bmatrix} 0 & 0 \\ 0 & \frac{-1}{RC} \end{bmatrix} & A_2 &= \begin{bmatrix} 0 & \frac{-1}{L} \\ \frac{1}{C} & \frac{-1}{RC} \end{bmatrix} & B_1 &= B_2 = \begin{bmatrix} \frac{1}{L} \\ 0 \end{bmatrix} \\
C &= \begin{bmatrix} -k_1 & -k_2 \end{bmatrix} & D &= \begin{bmatrix} 0 & 1 \end{bmatrix} & E_1 &= E_2 = \begin{bmatrix} 0 & 1 \end{bmatrix}
\end{aligned}
$$

The periodic solution calculated using Eq. (8) is shown in Fig. 11. The closed-loop poles calculated from Eq. (16) are $\sigma(\Phi) = 0.8 \pm 0.45i$, which are inside the unit circle. So the periodic solution is *locally* orbitally stable. The magnitude of the eigenvalues is 0.9225, indicating that the settling time to the steady state may be long. For example, let the initial state be $(i_L, v_C)' = (0.9, 8)'$. The simulated output voltage is shown in Fig. 12. After the transient, the state trajectory goes to the periodic solution.

The averaging method also predicts local stability (but not local *orbital* stability). From Section 2.7, the closed-loop poles predicted by the averaging method are

$$\sigma(\mathcal{A}) = (-0.2759 \pm 2.9276i) \times 10^5 \tag{60}$$

and $e^{\sigma(\mathcal{A})T} = 0.7887 \pm 0.5230i$, close to the eigenvalues found above using by the sampled-data method.

However, the circuit is not globally stable and is described in [9] as being unstable based on simulation. Since the averaging method is for local (small-signal) analysis, it is not surprising that it cannot predict lack of global stability.

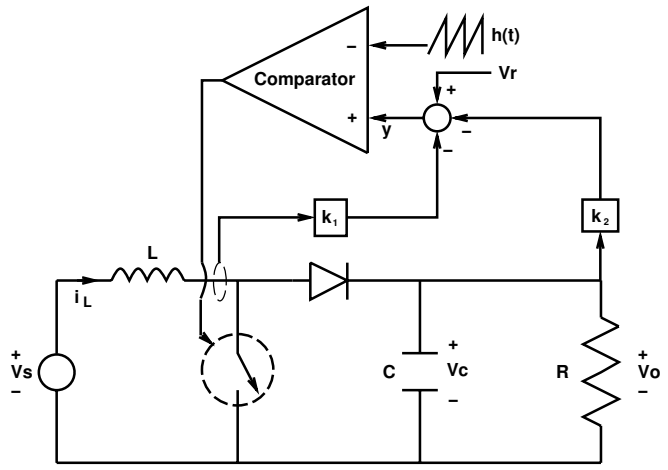

Figure 10: System diagram for Example 1

Example 2 (*Buck converter under voltage mode phase-lead control*, [15, p. 346]) The system diagram is shown in Fig. 13. The system parameters are as follows: $T = 10\mu s$, $V_s = 28V$, $R = 3\Omega$,

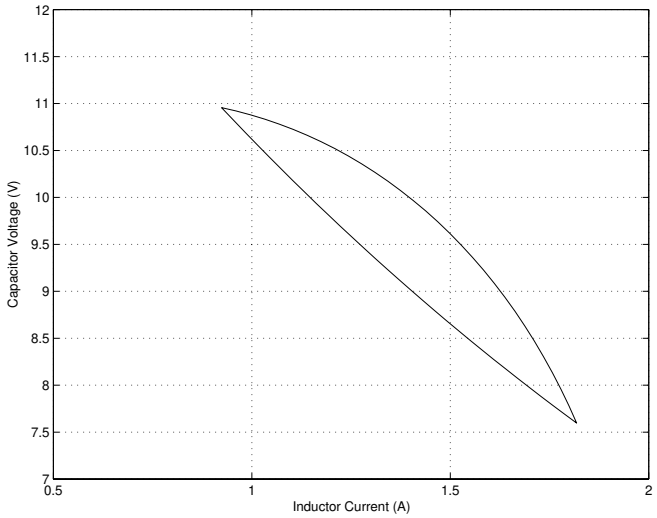

Figure 11: Periodic solution in Example 1

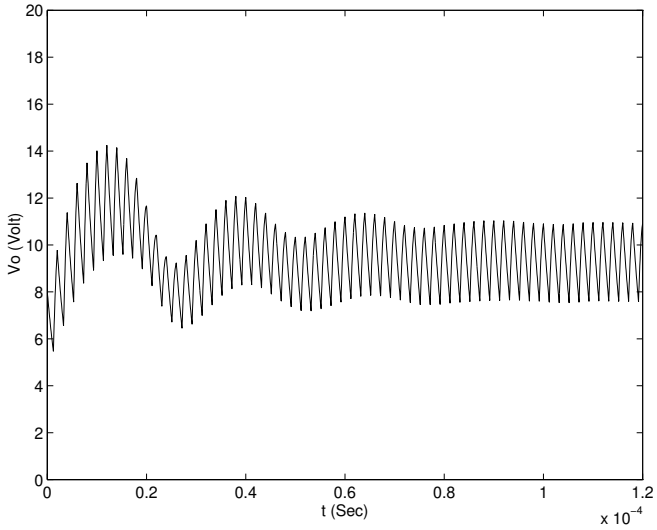

Figure 12: Output voltage trajectory in Example 1 for initial condition $(i_L, v_C)' = (0.9, 8)'$

$L = 50\mu H$, $C = 500\mu F$, $V_r = 5V$, $G_{c0} = 3.7$, $\omega_z = 10681\ rad/sec$, $\omega_p = 91106\ rad/sec$, and $h(t) = 4(\frac{t}{T} \bmod 1)$. The voltage divider gain g_{vd} is chosen to be 0.29465 (instead of 1/3 in [15]) to result in an output voltage at $15V$.

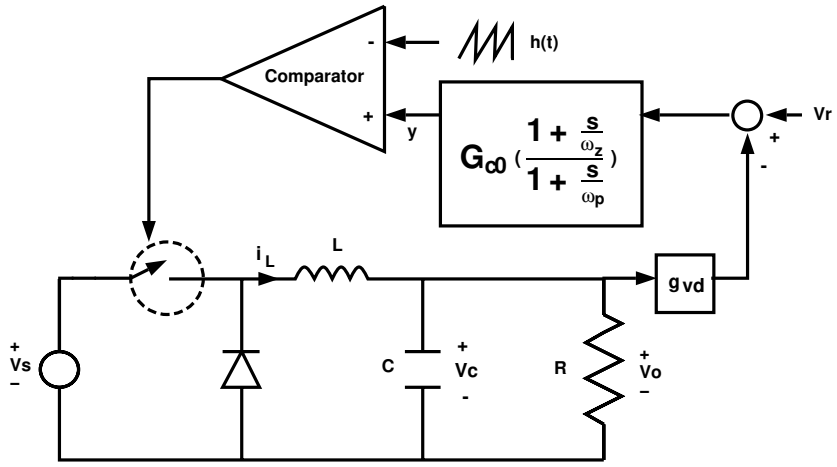

Figure 13: System diagram for Example 2

Let the state $x = (i_L, v_C, x_c)'$, where x_c is the state of the error amplifier. In terms of the representation in Fig. 3, one has

$$
\begin{aligned}
A_1 &= A_2 = \begin{bmatrix} 0 & \frac{-1}{L} & 0 \\ \frac{1}{C} & \frac{-1}{RC} & 0 \\ 0 & g_{vd}(\omega_p - \omega_z) & -\omega_p \end{bmatrix} \\
B_1 &= \begin{bmatrix} \frac{1}{L} & 0 \\ 0 & 0 \\ 0 & \omega_z - \omega_p \end{bmatrix} \qquad B_2 = \begin{bmatrix} 0 & 0 \\ 0 & 0 \\ 0 & \omega_z - \omega_p \end{bmatrix} \\
C &= \frac{G_{c0}\omega_p}{\omega_z} \begin{bmatrix} 0 & -g_{vd} & 1 \end{bmatrix} \qquad D = \begin{bmatrix} 0 & \frac{G_{c0}\omega_p}{\omega_z} \end{bmatrix} \\
E_1 &= E_2 = \begin{bmatrix} 0 & 1 & 0 \end{bmatrix}
\end{aligned}
$$

Solving Eqs. (9) and (13) by Newton's method results in $x^0(0) = (4.3, 15, -0.512)'$ and $d = 5.36 \times 10^{-6}$. The eigenvalues of the closed-loop system can be obtained from $\sigma[\Phi]$ and they are 0.8096 ± 0.1154 and 0.5973. All of them are inside the unit circle, so the periodic solution $x^0(t)$ is asymptotically orbitally stable.

Example 3 (*Boost converter under current mode control with voltage loop closed*, [18]) The system diagram is shown in Fig. 14, where $f_s = 25kHz$, $V_s = 28V$, $R = 11.2\Omega$, $L = 195\mu H$,

$C = 2mF$, $R_1 = 47.5k\Omega$, $R_2 = 2.5k\Omega$, $R_s = 0.8125\Omega$, $R_f = 72.2k\Omega$, and $C_f = 0.23\mu F$. The reference voltage V_r and thus the duty cycle are varied. The system is analyzed for two situations: without slope compensation ($h(t) = 0$), and with slope compensation ($h(t) = (\frac{R_s V_s T}{5L})[\frac{t}{T} \bmod 1]$).

Let the state $x = (i_L, v_C, v_{cf})'$. The system matrices in Fig. 3.1 are

$$
\begin{array}{rclcrcl}
A_1 & = & \begin{bmatrix} 0 & 0 & 0 \\ 0 & \frac{-1}{RC} & 0 \\ 0 & \frac{-1}{C_f R_1} & 0 \end{bmatrix} & & A_2 & = & \begin{bmatrix} 0 & \frac{-1}{L} & 0 \\ \frac{1}{C} & \frac{-1}{RC} & 0 \\ 0 & \frac{-1}{C_f R_1} & 0 \end{bmatrix} \\
B_1 & = & B_2 = \begin{bmatrix} \frac{1}{L} & 0 \\ 0 & 0 \\ 0 & \frac{1}{C_f R_1} + \frac{1}{C_f R_2} \end{bmatrix} & & & & \\
C & = & \begin{bmatrix} -R_s & \frac{-R_f}{R_1} & 1 \end{bmatrix} & & D & = & \begin{bmatrix} 0 & 1 + \frac{R_f}{R_1} + \frac{R_f}{R_2} \end{bmatrix} \\
E_1 & = & E_2 = \begin{bmatrix} 0 & 1 & 0 \end{bmatrix} & & & &
\end{array}
$$

First, consider the system without slope compensation. The duty cycle is varied (for different V_r) from 0.4 to 0.6 and $\sigma[\Phi]$ is plotted and shown in Fig. 15. One eigenvalue trajectory crosses the unit circle at $D_c = 0.498$. The other two remain very close to 1. For $D_c > 0.498$, the system is unstable.

Next, consider the system with slope compensation. The duty cycle is varied from 0.4 to 0.7 and $\sigma[\Phi]$ is calculated. One eigenvalue trajectory crosses the unit circle at $D_c = 0.5845$. For $D_c > 0.5845$, the system is unstable.

In [18], the system is reported to be unstable for $D_c > 0.454$ without slope compensation and for $D_c > 0.61$ with slope compensation.

Example 4 (*Boost converter under current mode control*, [19]) Consider the same boost converter as in Example 3, with the following differences: here $f_s = 100kHz$, $V_r = 1.8V$, $h(t) = 0$ and parasitic resistances in the switch, diode, inductor, and capacitor are modeled and are given by $R_Q = 0.055\Omega$, $R_D = 0.011\Omega$, $R_I = 0.03\Omega$, $R_c = 0.012\Omega$, respectively. With these choices, the system is studied in [19] and shown to be stable. However, both state-space average model and an improved model [20] predict the system to be unstable.

Let the state $x = (i_L, v_C, v_{cf})'$. As in [19], let $\alpha = R/(R + R_c)$ and $\beta = \alpha R_c$. The system

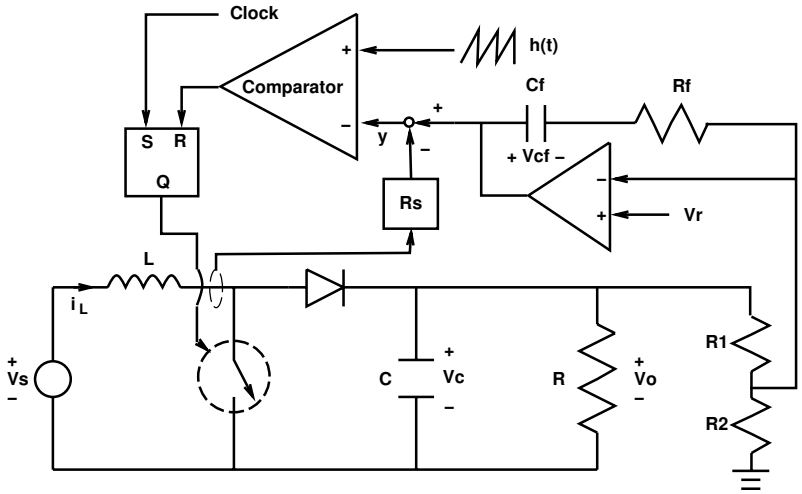

Figure 14: System diagram for Example 3

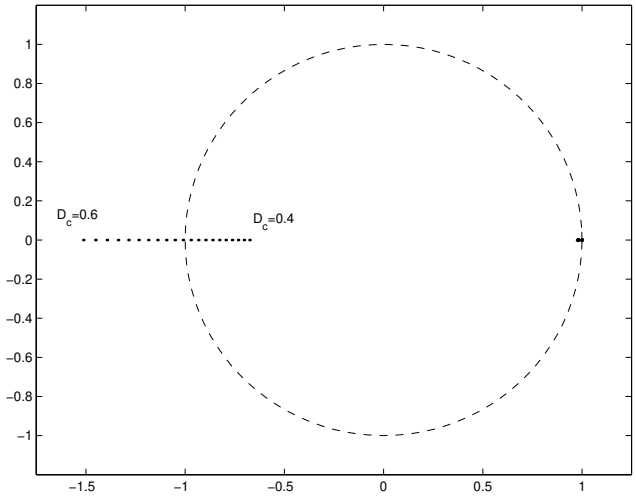

Figure 15: $\sigma(\Phi)$ as D_c varies from 0.4 to 0.6

matrices in Fig. 3.1 are

$$A_1 = \begin{bmatrix} \frac{-(R_I+R_Q+R_s)}{L} & 0 & 0 \\ 0 & \frac{-1}{(R+R_c)C} & 0 \\ 0 & \frac{-\alpha}{C_f R_1} & 0 \end{bmatrix} \qquad A_2 = \begin{bmatrix} \frac{-(R_I+R_D+\beta)}{L} & \frac{-\alpha}{L} & 0 \\ \frac{\alpha}{C} & \frac{-1}{(R+R_c)C} & 0 \\ \frac{-\beta}{C_f R_1} & \frac{-\alpha}{C_f R_1} & 0 \end{bmatrix}$$

$$B_1 = B_2 = \begin{bmatrix} \frac{1}{L} & 0 \\ 0 & 0 \\ 0 & \frac{1}{C_f R_1} + \frac{1}{C_f R_2} \end{bmatrix}$$

$$C = \begin{bmatrix} -R_s & \frac{-R_f \alpha}{R_1} & 1 \end{bmatrix} \qquad D = \begin{bmatrix} 0 & 1 + \frac{R_f}{R_1} + \frac{R_f}{R_2} \end{bmatrix}$$

$$E_1 = \begin{bmatrix} 0 & \alpha & 0 \end{bmatrix} \qquad E_2 = \begin{bmatrix} \beta & \alpha & 0 \end{bmatrix}$$

The closed-loop poles ($\sigma[\Phi]$) are calculated as -0.3383, 0.9928 and 0.9994. Thus, the sampled-data approach gives a better indication of stability than the averaged model.

5 Concluding Remarks

General sampled-data modeling and analysis were performed for closed-loop PWM DC-DC converters. The models unify past work, while removing simplifying approximations. They apply both for current mode control and voltage mode control. Linearized models were derived analytically, and used to perform associated calculations, among which are general results on stability. Examples were used to show that the sampled-data approach will reliably predict the (local) stability of a converter for which averaging or simulation predicts instability. Thus, sampled data models should be viewed as an important tool for closed-loop performance validation. It is hoped that this work will help to facilitate further applications of the sampled-data approach in power electronics.

Acknowledgments

This research has been supported in part by the the Office of Naval Research under Multidisciplinary University Research Initiative (MURI) Grant N00014-96-1-1123, the U.S. Air Force Office of Scientific Research under Grant F49620-96-1-0161, and by a Senior Fulbright Scholar Award.

References

[1] F.C.Y. Lee, R.P. Iwens, Yuan Yu, and J.E. Triner, "Generalized computer-aided discrete time-domain modeling and analysis of DC-DC converters," *IEEE Transactions on Industrial Electronics and Control Instrumentation*, vol. IECI-26, no. 2, pp. 58–69, 1979.

[2] G.C. Verghese, M. Elbuluk, and J.G. Kassakian, "A general approach to sample-data modeling for power electronic circuits," *IEEE Transactions on Power Electronics*, vol. 1, no. 2, pp. 76–89, 1986.

[3] R. Lutz and M. Grotzbach, "Straightforward discrete modelling for power converter systems," in *IEEE Power Electronics Specialists Conference Record*, 1986, pp. 761–770.

[4] A.R. Brown and R.D. Middlebrook, "Sampled-data modelling of switching regulators," in *IEEE Power Electronics Specialists Conference Record*, 1981, pp. 349–369.

[5] J.H.B. Deane and D.C. Hamill, "Instability, subharmonics, and chaos in power electronics circuits," *IEEE Transactions on Power Electronics*, vol. 5, no. 3, pp. 260–268, 1990.

[6] D.C. Hamill, J.H.B. Deane, and J. Jefferies, "Modeling of chaotic DC-DC converters by iterated nonlinear mappings," *IEEE Transactions on Power Electronics*, vol. 7, no. 1, pp. 25–36, 1992.

[7] J.H.B. Deane, "Chaos in a current-mode controlled boost DC-DC converter," *IEEE Transactions on Circuits and Systems-I: Fundamental Theory and Applications*, vol. 39, no. 8, pp. 680–683, 1992.

[8] C.K. Tse, "Flip bifurcation and chaos in three-state boost switching regulators," *IEEE Transactions on Circuits and Systems-I: Fundamental Theory and Applications*, vol. 41, no. 1, pp. 16–23, 1994.

[9] B. Lehman and R.M. Bass, "Switching frequency dependent averaged models for PWM DC-DC converters," *IEEE Transactions on Power Electronics*, vol. 11, no. 1, pp. 89–98, 1996.

[10] R. Tymerski, "Frequency analysis of time-interval-modulated switched networks," *IEEE Transactions on Power Electronics*, vol. 6, no. 2, pp. 287–295, 1991.

[11] R. Tymerski, "Application of the time-varying transfer function for exact small-signal analysis," *IEEE Transactions on Power Electronics*, vol. 9, no. 2, pp. 196–205, 1994.

[12] C.-C. Fang, *Sampled-Data Analysis and Control of DC-DC Switching Converters*, Ph.D. thesis, University of Maryland, College Park, 1997, available at http://www.isr.umd.edu/TechReports/ISR/1997/.

[13] H.K. Khalil, *Nonlinear Systems*, Macmillan, New York, 1992.

[14] K. Ogata, *Discrete-Time Control Systems*, Prentice Hall, Englewood Cliffs, NJ, Second edition, 1995.

[15] R.W. Erickson, *Fundamentals of Power Electronics*, Chapman and Hall, New York, 1997.

[16] R.D. Middlebrook and S. Ćuk, "A general unified approach to modelling switching-converter power stages," in *IEEE Power Electronics Specialists Conference Record*, 1976, pp. 18–34.

[17] A.V. Oppenheim and R.W. Schafer, *Discrete-Time Signal Processing*, Prentice-Hall, Englewood Cliffs, NJ, 1989.

[18] I. Zafrany and S. Ben-Yaakov, "A chaos model of subharmonic oscillations in current mode PWM boost converters," in *IEEE Power Electronics Specialists Conference Record*, 1995, pp. 1111–1117.

[19] R.M. Bass, B.S. Heck, and R.A. Khan, "Average modelling of current-mode controlled converters: instability predictions," *International Journal of Electronics*, vol. 77, no. 5, pp. 613–628, 1994.

[20] F.D. Tan and R.D. Middlebrook, "A unified model for current-programmed converters," *IEEE Transactions on Power Electronics*, vol. 10, no. 4, pp. 397–408, 1995.